

Implementing Cellular Remodelling in Discrete Cell Models

Reuben van Ammers, Dr. James Osborne

Abstract. Epithelial monolayers, layers of tissue in the body one cell thick, have a large impact in many biological processes. Recently, it has been seen that in response to mechanical forces, monolayers often display non-elastic properties, particularly with responses displaying multiple distinct timescales due to cellular remodelling. Current discrete cell models, which are based on static parameters, do not exhibit these properties, and so we introduce a dynamic reference state in cell centre and cell vertex models in order to represent remodelling. Using this reference state, in appropriate parameter regimes, we find that we can observe the presence of multiple timescales and the desired mechanical properties of the discrete cells as a monolayer.

Submitted to: *Phys. Biol.*

1. Introduction

On the surfaces of many cavities and organs in the human and animal body, there exist many epithelial sheets of cells [10]. Many of these layers of epithelial cells are “simple”, being one cell layer thick, and are called *monolayers*. These monolayers are often subjected to mechanical forces, and therefore understanding how these cells react in the face of these forces is paramount in understanding these phenomena. Cell proliferation in the intestinal crypt produces forces which result in cell migration [4]. Inside the lung, pulmonary alveoli deform due to changing pressures during breathing, causing deformation of the one cell thick alveoli [14]. Monolayers are subjected to various forces during embryonic development, influencing morphogenesis [13]. To understand these systems better, we want to explore how these monolayers behave experimentally, and ultimately to be able to reproduce these properties computationally to perform *in silico* experiments.

1.1. Experimental Results and the Presence of Multiple Timescales

In 2011, Harris et al. [7] investigated experimentally the mechanical properties of an epithelial monolayer. To do this, they connected the edges of a cell monolayer to a set of rods, one of which was held fixed, and the other one which could be moved. Using these two rods, a variety of mechanical experiments were undertaken, where forces were applied to the dynamic rod and the resulting behaviour of the monolayer was recorded.

These monolayers at equilibrium were around 1mm in length and height, meaning that each of the monolayers experimented upon were only a few hundred cells long and high. This is a relatively small amount of cells, meaning that the small scale behaviour of these monolayers could be investigated.

A variety of different experiments were presented in this paper, but we will focus on two of them: the creep experiment and the stress relaxation experiment, as these are two of the most critical experiments in categorising the behaviour of viscoelastic materials.

In the creep experiment, the left side of the monolayer is held fixed, while the right side of the monolayer has a constant force applied to the rod attached to the monolayer, stretching the monolayer. The length of the monolayer is then recorded, and the strain, the resultant length divided by the initial length, is recorded over time.

In the stress relaxation experiment, the monolayer is pulled to the right at a constant rate and then held. The resulting force to the left, the stress, is then recorded over time.

In the resulting curves obtained from these experiments, we see the distinct presence of multiple timescales, where the monolayer produces clearly different behaviour at different times. In the creep experiment (Figure 1a), the monolayer rapidly extends initially, followed by a slow increase in length as the applied force is maintained. The effect of this becomes more prominent as the force applied to the monolayer is increased.

In the stress relaxation experiment (Figure 1 (b,c)), we also see differing behaviour of the resulting stress-time curves in response to different magnitudes of external influence, in this case the strain-rate of loading. Slow initial loading produces stress-time graphs that can be accurately described as exponential behaviour. On the other hand, after high strain-rate loading, we initially see a relatively quick drop off in stress, followed by a slow decrease as time increases.

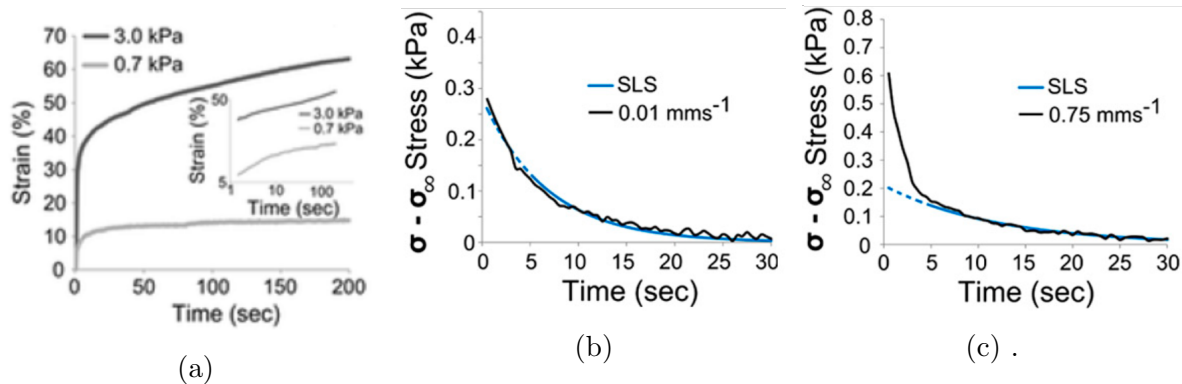


Figure 1: (a) Strain vs time of a biological monolayer in response to external stress.(b,c) Stress vs time following low and high strain-rate loading respectively for a stress relaxation experiment. Figures reproduced from Harris et al. [7]

1.2. Mathematical Models of Tissue Deformation

In standard models of viscoelastic materials, such as the standard linear solid (SLS) model, we expect the creep and stress relaxation responses to follow exponential behaviour [6]. The deviation of these responses from simple mechanical models, despite the inherent simplicity of a monolayer compared to other biological tissues, suggest that something more complicated is in play. For tissue deformation over a long period of time, with nutrients available, one might surmise that the increase in strain is due to cell growth, or the movement of cells within the monolayer in order to react to the mechanical forces. However neither of these processes were observed in the above experiment, due to the short duration of the experiment .

There exist two main ways of describing biological tissue: from a continuum tissue based perspective or a discrete cell based perspective [9]. In this paper, we will be focusing on the cell based alternative, as this allows small scale behaviour to be observed. There exist many different mathematical models for describing cells, with applicability being dependent on the situation being modelled [12].

One large class of discrete cell based models are cell centre based models, wherein the location of cells are described as a single point each, the center of the cell. Forces due to external factors, as well as interactions between cells, are applied to these . One manner in which interconnectivity between cells can be expressed is as an initial fixed

connectivity, with the connectivity often chosen initially with a Delaunay Triangulation [2]. Another common method for representing the connectivity is having two cells being connected if they are sufficiently close together, with connectivity being able to change due to movement of the cell centers, known as the overlapping spheres model [9]. When cells are connected, they are modelled as having a potential between them, often a spring potential between cell centers with a preferred length.

One other large class of models describe cells as polygons, with these polygons being fully described by the vertices [5]. The choice of polygons as the shape of the cells is motivated by experimental data, with cross sections of epithelial cells showing polygonal structures [8]. These vertex based models usually allow a bit more flexibility in describing systems in comparison to cell centre models due to their higher degrees of freedom [1].

1.3. A Cell Centre Model for Monolayer Deformation

We now describe explicitly the mechanics of an example of one of the more common class of cell models, the discrete cell centre model. For calculating the movement directly, the dynamics of the system is usually taken to be overdamped so that inertial movement is ignored, leaving only movement due to forces [3]. Taking the drag coefficient as γ_r , this gives us the equation of motion

$$\gamma_r \frac{d\mathbf{r}_i}{dt} = \mathbf{F}_i.$$

In the following, we will base our cell centre model on the linear spring model, using the triangulation method of connectivity and finding the movement of cells based by solving the ODEs produced by the forces. This can be represented in the following equation:

$$\gamma_r \frac{d\mathbf{r}_i}{dt} = \sum_{j \in N_i} k(||\mathbf{r}_{ij}|| - s_{ij}) \hat{\mathbf{r}}_{ij} + \mathbf{F}_i^{\text{applied}}, \quad (1)$$

where \mathbf{r}_i is the location of cell centre i , $\mathbf{r}_{ij} = \mathbf{r}_i - \mathbf{r}_j$, N_i is the set of cells connected to cell i , s_{ij} is the equilibrium distance between the centres of cells i and j , k is the spring constant, γ_r is the drag coefficient and $\mathbf{F}_i^{\text{applied}}$ is the external force applied to cell i .

There exists a wealth of different force functions, some of which have been described in this section, and many of these become increasingly complicated as they further attempt to match observed biological behaviours [12]. However, in bulk systems, these different force functions tend to exhibit similar elastic behaviours, at least in simulations wherein cell connectivity remains constant [12]. There have been some attempts at including the viscous type of effects seen experimentally. One of these has been in the work of J. Munoz and Santiago Albo [11], where the rest length between cells i and j can change in a manner proportional to the strain of the cells:

$$\frac{\dot{s}_{ij}}{s_{ij}} \propto \frac{\| \mathbf{r}_{ij} \| - s_{ij}}{s_{ij}},$$

producing deformation of cell lengths in a manner similar to the Maxwell viscoelastic model. This change in cell lengths is permanent however, on release of the external force, and cell lengths increase infinitely with continued applied stress, making it unsuitable for representing the behaviour of the creep experiment.

The remainder of this paper is structured as follows. First, we propose a novel model of discrete cell interactions, where we have a dynamic reference state to capture the multiple timescale behaviour observed in Harris et al. [7]. We then describe a method to determine the extent of multiple timescale behaviour from a given simulation. We then perform simulations over a variety of parameters to determine the presence of multiple timescale behaviour in the new model for the creep and stress relaxation experiments. Finally, we propose an extension to our model, wherein we introduce the concept of "memory" and an extra associated timescale and examine its effects on cell behaviour.

2. A Multicellular Framework For Cellular Remodelling

In this section, we propose a method to represent cellular remodelling within the cell centre linear spring framework described previously. Various mechanical experiments will be performed, and the effects of various parameters on the model will be explored. These results will then be compared to the experimental data in Harris et al. [7], and the suitability of the model for the description of empirical phenomena will be discussed.

2.1. Evolving Reference State

We begin by making some definitions. We define the set of cells that are affected by external forces as the *real state*. This state encodes information about cells that have a direct physical meaning; in the cell centre model, the real state is characterised by the set of cell centres. Under this definition, the data modelled under previous cell descriptions would have been in the real state.

To contrast with this, we introduce the *reference state*. Unlike the real state, this state does not have a direct physical meaning; it cannot be affected directly by external forces or be observed to see the outcome of some experiment. Rather, the reference state will encode information to inform the behaviour of the real state. Information from the real state will be able to influence the reference state, and information from the reference state will be able to influence parameters of the real state. In doing so, the aim is to allow properties of the cells, captured in the reference frame, to change over time in response to the application of external forces.

In order to simulate the remodelling, we need two sets of variables, the location of 'real' cell centres and location of 'reference' cell centres. For each cell centre, the location of which is labelled \mathbf{r}_i , we have a corresponding reference cell centre, denoted

as ρ_i . We assume that the reference and real cell centres have the same connectivity as each other; extensions will be explored in the discussion.

In the simple cell centre linear spring model, we have that forces are modelled as linear springs, with forces in the real state being determined via intercellular distances. We use similar ideas with the addition of the reference state, but the equilibrium spring between two cell centres is no longer static, but rather determined as the distance between the corresponding cells in the reference state. The reference cells on the other hand are modelled as being effected by two different sources. Firstly, between two reference cells there is a linear spring component with equilibrium length equal to the intercellular distance between the corresponding real cells, allowing the reference cells to move due to movement in the real state. Secondly, there is a spring force between reference cells with a static equilibrium length, representing the natural length between reference cells.

To incorporate the evolving reference frame into the cell centre model, we modify the set of equations in the standard cell model of Equation (1) as follows:

$$\gamma_r \frac{d\mathbf{r}_i}{dt} = \sum_{j \in N_i} k(||\mathbf{r}_{ij}|| - ||\rho_{ij}||) \hat{\mathbf{r}}_{ij} + \mathbf{F}_i^{\text{applied}}, \quad (2)$$

$$\gamma_\rho \frac{d\rho_i}{dt} = \left(\sum_{j \in N_i} k_S(||\rho_{ij}|| - s_0) \hat{\rho}_{ij} + \sum_{j \in N_i} k_R(||\rho_{ij}|| - ||\mathbf{r}_{ij}||) \hat{\rho}_{ij} \right), \quad (3)$$

where as before $\mathbf{r}_{ij} = \mathbf{r}_i - \mathbf{r}_j$ and $\rho_{ij} = \rho_i - \rho_j$. We denote the drag coefficients for the real and reference states as γ_r and γ_ρ respectively. The spring constants referring to the real state, static component of the reference state and remodelling component of the reference state are denoted as k , k_S and k_R respectively.

Following this definition, we non-dimensionalise Equations (2) and (3). We non-dimensionalise the terms in the above equations:

$$\tilde{\mathbf{r}}_i = \frac{\mathbf{r}_i}{s_0}, \quad \tilde{\rho}_i = \frac{\rho_i}{s_0}, \quad \tilde{\mathbf{F}}_i^{\text{applied}} = \frac{\mathbf{F}_i^{\text{applied}}}{ks_0}, \quad \tilde{t} = \frac{kt}{\gamma_r}.$$

We also define the following non-dimensional parameters:

$$\alpha = \frac{k_S}{k_R + k_S}, \quad \eta = \frac{\gamma_r}{\gamma_\rho} \frac{k_R + k_S}{k}.$$

After we substitute, simplify and then drop the tildes for notational simplicity we have:

$$\frac{d\mathbf{r}_i}{dt} = \sum_{j \in N_i} (||\mathbf{r}_{ij}|| - ||\rho_{ij}||) \hat{\mathbf{r}}_{ij} + \mathbf{F}_i^{\text{applied}}, \quad (4)$$

$$\frac{d\rho_i}{dt} = \eta \left(\alpha \sum_{j \in N_i} (||\rho_{ij}|| - 1) \hat{\rho}_{ij} + (1 - \alpha) \sum_{j \in N_i} (||\rho_{ij}|| - ||\mathbf{r}_{ij}||) \hat{\rho}_{ij} \right), \quad (5)$$

which shows we can completely characterise the behaviour of the model via these two parameters α and η . The parameter α determines the relative strength between the static and remodelling components of the reference state dynamics, and η determines the speed of movement of the reference state in comparison to the real state. We define α to be the remodelling ratio, and η as the remodelling rate.

In this work, all experiments were undertaken on a 10 by 10 hexagonal grid of cells initially at equilibrium (shown in Figure 2) chosen to balance realism with computational constraints.

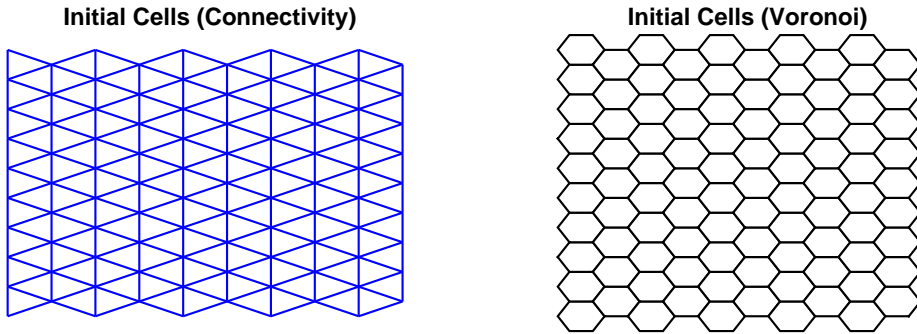


Figure 2: Initial cell configuration for all experiments is a 10 by 10 hexagonal grid, for both the real and reference cells.

2.2. Creep Response & Stress Relaxation Experiment

In order to assess the properties of this model, *in silico* versions of creep experiment and stress relaxation experiments were performed, and results compared to previous models.

For the creep experiment, a constant stress was applied to right side of the cells. We define this stress as F_{ext} , which is expressed mathematically as setting $\mathbf{F}_i^{\text{applied}}$ as a vector of magnitude F_{ext} to the right for the set of rightmost cells. The left side of the monolayer was held fixed. In this experiment the strain vs time of the monolayer was recorded. The simulation was set to stop if the strain value went above a threshold s_{\max} during the calculation. We chose $s_{\max} = 5$ to avoid overly unrealistic strains. This is above the value that the creep experiment in Harris et al. [7] failed at, but this failure was due to delamination of the monolayer with the testing rods, so a slightly higher value was chosen here. An example of the strain over time of such a simulation is shown in Figure 3a.

For the stress relaxation experiment, the left side of the cells were held fixed, while the right hand edge was pulled such that the strain of the monolayer increased up to maximum length (set as 1.5 times the original length, due to being in the range of strain values measured in Harris et al. [7]) at a constant rate of strain, and then held at that length. We will call the time it takes for monolayer to be pulled to the maximum strain the *ramp time*, and denote it T_{ramp} . Immediately after the monolayer stops, it was held at the constant strain of 1.5 and we recorded the stress felt at the right edge of the

monolayer. The stress-time graph of such an experiment is shown in Figure 3b.

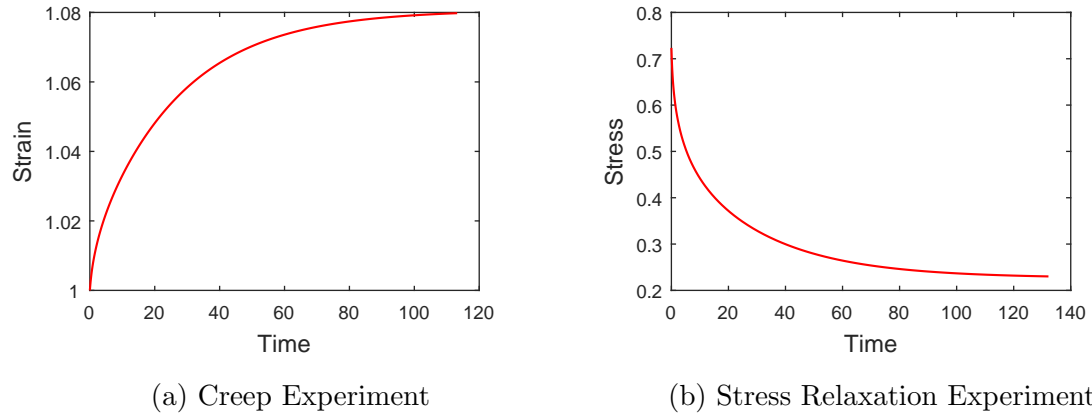


Figure 3: Example of a strain-time graph for the creep experiment and a stress-time graph for the stress relaxation experiment.

2.3. Multiple Relaxation Timescales

As is the case with experimental results, it can be observed that there was often two different regions in the plots for both the creep and stress relaxation experiments wherein distinct exponential regions can be distinguished. To capture this behaviour in our simulations we fit the results with both single and double exponentials (i.e., a sum of two exponentials).

In order to compare error values between graphs without bias, the y values (stress or strain) of all of the graphs were rescaled to fit between 0 and 1. The data was then fitted with both one exponential and two exponential fits,

$$y_1 = A_1 + B_1 e^{-\frac{t}{\tau_1}}, \quad (6)$$

$$y_2 = A_2 + B_{21} e^{-\frac{t}{\tau_{21}}} + B_{22} e^{-\frac{t}{\tau_{22}}}, \quad (7)$$

where without loss of generality we choose $\tau_{21} \leq \tau_{22}$.

We restrict the values of the τ variables to be positive in order to represent exponential decay over time as the system reached a steady state (as seen in Figure 3). In addition, we require the sign of B_{21} and B_{22} to be the same (negative for the creep experiment and positive for the stress relaxation experiment) so that the calculated exponentials in the two timescale fit correspond to aspects of the decay in the graph, and not a “lucky” cancellation of a positive and negative exponentials.

Examples of the results of such fits, with differing parameters, can be seen in the top half of Figures 4 and 5, representing examples from the creep and stress relaxation experiments respectively. Note that the two exponential fit in blue will always better than (or equal to) a single exponential fit. We can see the green line (the short timescale component of the two exponential fit) fits the data relatively well for short times, and the yellow line (the long timescale component of the two exponential fit) fits the data

relatively well for long times, indicating the two separate timescale realms. We can see Figs 4b and 5b have a greater contribution by the short timescale, and thus can less effectively be represented by a single exponential curve. This can be seen in Figures 4d and 5d where the errors on the right for the creep and stress relaxation examples have significantly larger errors with a one exponential fit than for a two exponential fit.

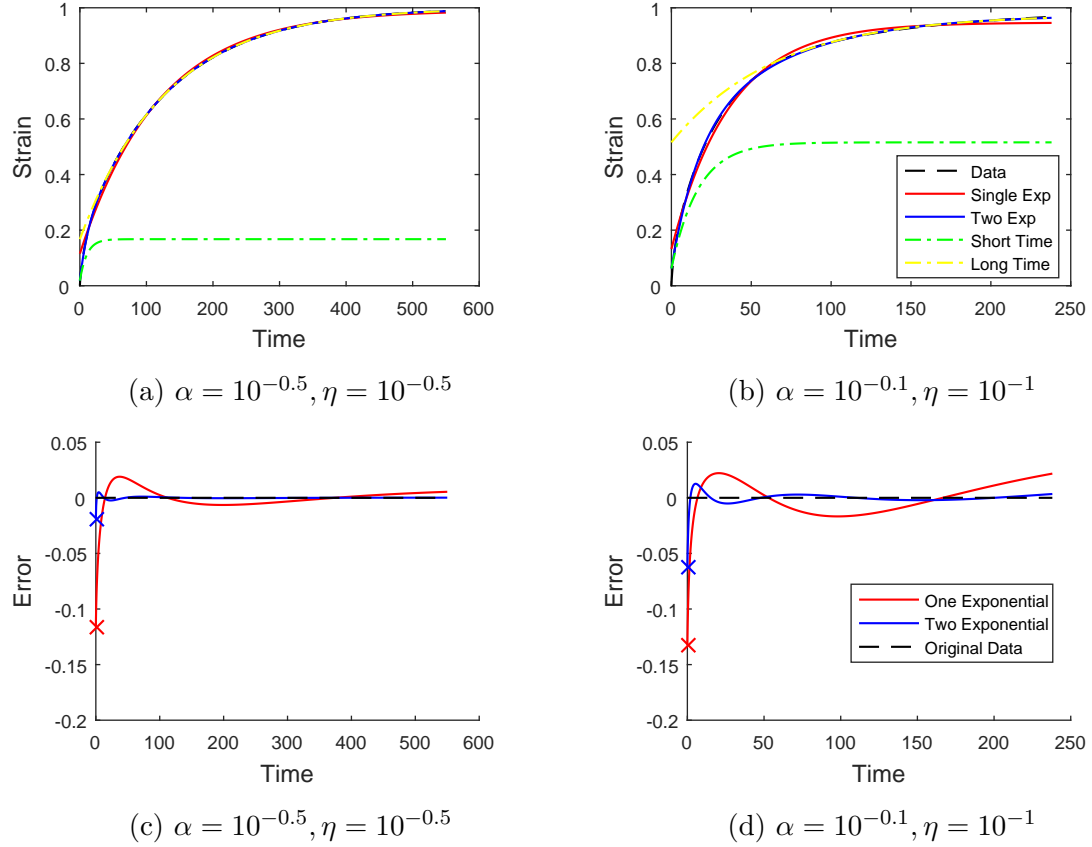


Figure 4: Top: Examples of a fit of a strain-time curve from the creep experiment for specific parameters. Bottom: Error values for the above plots for each exponential fit. Note the significantly better accuracy for the two exponential fit.

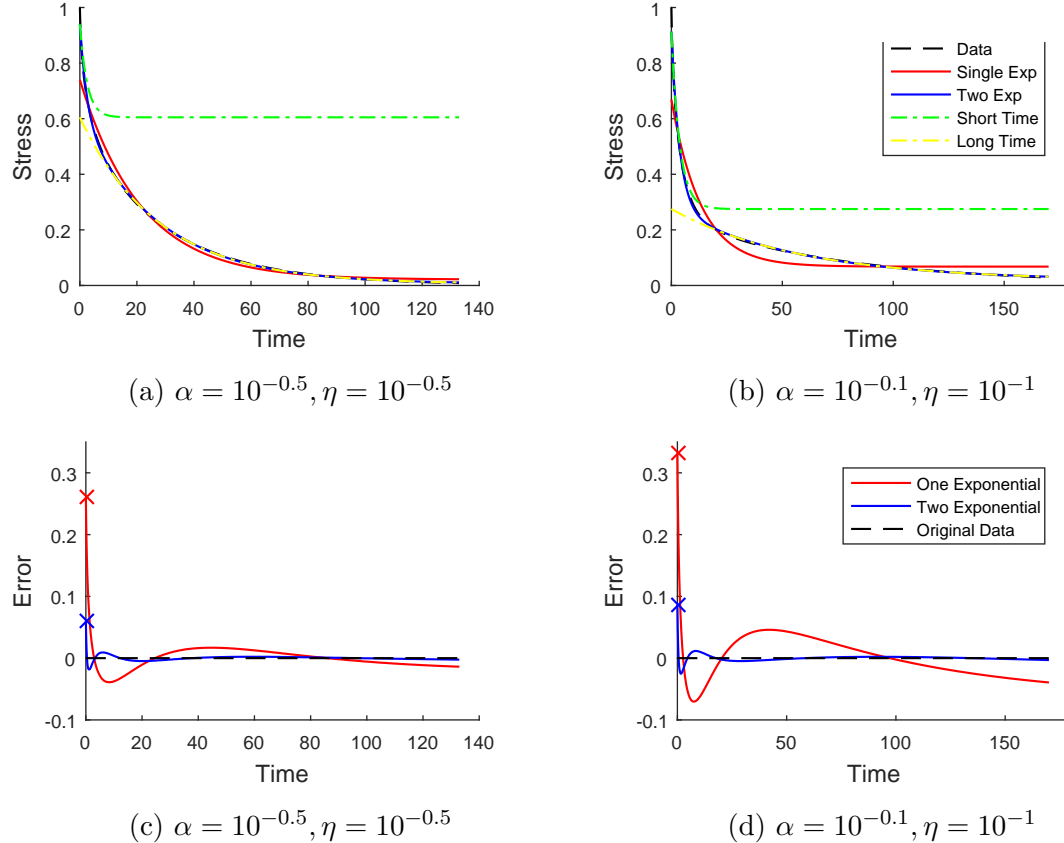


Figure 5: Top: Examples of a fit of a stress-time curve from the stress relaxation experiment. Bottom: Error values for the above plots for each exponential fit. Note the significantly better accuracy for the two exponential fit.

The presence of remodelling appears to introduce an extra timescale into the problem that can be captured by the second exponential. In order to make effective comparisons between the simulation data, we require a comparison between one and two exponential fits which measures the presence of multiple timescales.

2.4. Timescale Metric

When fitting the data with the exponential type fits as in Equations (6) and (7), we have that the long exponential timescale τ_{22} will always be greater than the single exponential timescale τ_1 . The closer these two values, the better the graph can be fully represented by a single exponential. Therefore, we use the ratio of the long two exponential timescale τ_{22} and the timescale of the single exponential τ_1 , as a metric for the amount of two timescale behaviour of the data.

We define the coefficient ratio:

$$\tau_r = \frac{\tau_{22}}{\tau_1}. \quad (8)$$

For example, in Figure 5a where the one exponential model is a good fit, we have $\tau_1 = 21.45$, $\tau_{21} = 2.55$ and $\tau_{22} = 27.80$. This gives a coefficient ratio of

$$\tau_r = \frac{\tau_{22}}{\tau_1} = \frac{27.80}{21.45} = 1.29.$$

In Figure 5b, where the one exponential description is less accurate, we have that $\tau_1 = 13.40$, $\tau_{21} = 3.73$ and $\tau_{22} = 58.21$, giving a coefficient ratio of

$$\tau_r = \frac{\tau_{22}}{\tau_1} = \frac{58.21}{13.40} = 4.34.$$

We see in this example that τ_r gives a numerical value to the presence of multiple timescale behaviour, with larger values representing a higher presence of two timescale behaviour.

3. Results

3.1. The Effect of Remodelling Ratio and Remodelling Rate on Timescales

To analyse the possible behaviour of our model, the parameters α and η were swept over for both the creep and stress relaxation experiment. The values of α and η that were swept over were both between 0.1 and 1, one order of magnitude difference.

3.1.1. Creep Experiment In Harris et al. [7], increasing the force on the monolayers increased the presence of two exponential behaviour. In the sweep of the creep experiment, we increased the external force F_{ext} to see if force variations changed the simulation's multiple timescale behaviour. F_{ext} was swept over the values 10^{-1} , $10^{-0.5}$, and 10^0 .

Some examples of the strain-time graphs and results of exponential fitting to them are presented in the Figure 6 (c,d,e) insets.

Figure 6 (a,b), presents how timescale coefficients change for varying α and η values. The blue and black dots represent the long (τ_{22}) and short (τ_{21}) timescales, respectively, of the fits of the data, while the red dots are the timescale of the one exponential fit (τ_1). The red dots of the single exponential timescale were fixed at a constant size. The size of the black and blue dots are scaled by the magnitude of the exponential term relating to the timescale B_{21} and B_{22} respectively. If one of the exponentials is smaller magnitude than the other, then it will have a correspondingly smaller dot, while the other will remain at the same size as the red dot. Notice that the one exponential attempts to compromise between the long and short timescales of the exponential and therefore we see that the single timescale lies between the two timescales for the two exponential fit.

In Figure 6 (c,d,e), the plots show the errors between the data and the fits of the data, representative of the behaviour of the system in different regions. The error of the one exponential fit is shown in black, while the error of the two exponential fit is shown in blue. The insets show the original data, overlaid with the different exponential fits. The black dots are the original data, the red line is the one exponential fit and the blue line is the two exponential fit.

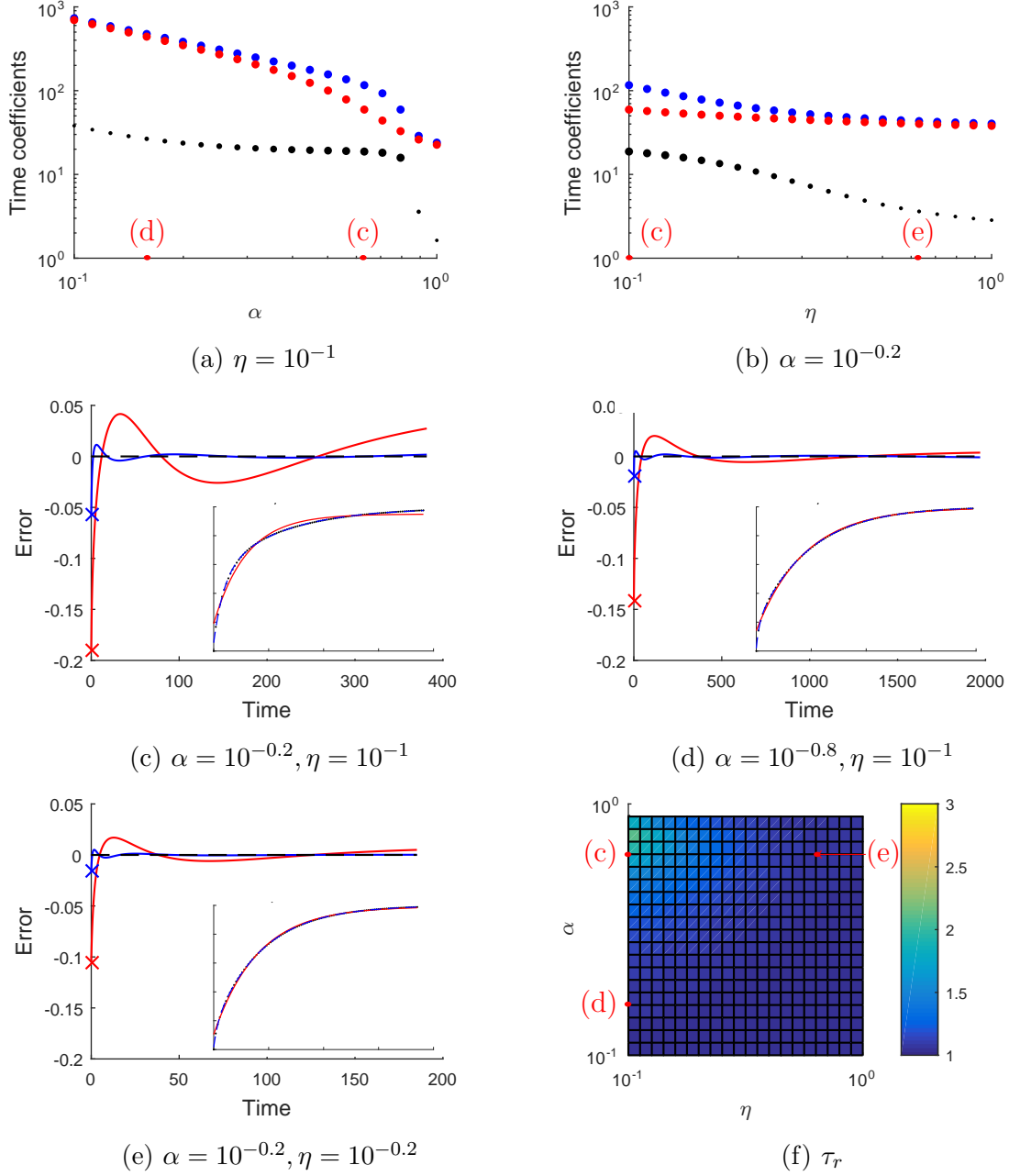


Figure 6: Example time differences for the creep experiment. All plots were taken with values of $F_{\text{ext}} = 10^{-0.5}$. (a,b) Displays values of τ_1 (red), τ_{21} (black) and τ_{22} (blue), where dot size for τ_{21} and τ_{22} are scaled by B_{21} and B_{22} respectively. (c,d,e) Displays error values for two exponential fit (blue), one exponential fit (red) in comparison to the data (black), with inset strain-time plots showing the original data with the same respective colour scheme. (f) Represents τ_r as surface plot over different η and α values.

Figure 6f shows τ_r as surface plot, varying over both η and α . The $\alpha = 1$ components of the graph have been removed from the graph, as they are a degenerate case displaying no remodelling.

In Figure 6a, we can see that as α decreases, the long timescale τ_{22} (blue) increases in magnitude by a large amount, while the short timescale τ_{21} (black) only increases slightly. This is consistent with the explanation of the reference cells' movement contributing to the long time behaviour of the system, with decreasing α causing the reference state to have greater movement, and thus affecting the long time behaviour of the system. However, at low times, this remodelling doesn't have enough time to take effect, and so the smaller timescale (black) is largely unaffected.

Similarly, in Figure 6b, we can see the effect of varying the remodelling rate η . At high values of η , the long and the one exponential timescales are similar, and get increasingly differentiated as we decrease the remodelling ratio, meaning that the behaviour can be better described as biexponential behaviour for low remodelling rates. This can be understood as at low values of η it takes time for the reference state to be affected by the force changing the distance between cell centres. This allows the real state to initially move at a timescale largely divorced from the effects of the reference state, due to the reference state being effectively static over those periods of time. We then get a long timescale resulting from the movement of the reference state allowing further strain of the real monolayer. However, at large values of η , the two states effectively act in concert, with movement of the real state quickly causing a change in the reference state. This "blurs" the effect of the cellular remodelling and results in largely single timescale behaviour.

We can see an example of this where there is a large differences in timescales in Figure 6c. The data (black) has large variation with the one exponential fit (red), and can be much better approximated a sum of exponentials (blue). This can be seen in the inset strain-time graphs as having a noticeable kink, which is representative of simulations exhibiting multiple timescales.

We will tend to get the greatest presence of biexponential behaviour if effects from the external force acting on the real cells as well as the effects from interactions between the real and reference cells are both of similar magnitude. Therefore, we get the largest effects at low values of η , when the two regions can clearly be distinguished, and at relatively high values of α , when the initial behaviour not due to the dynamic nature of the reference state is a non-negligible component. This can be seen in 6f as the bright region at the top left corner of the surface plot.

We can see the small amount of multiple timescale behaviour with no remodelling, by looking at when α equals one. This can be seen in Figure 6a in the regions of high α . We can see that timescale of the system with no remodelling (corresponding to α equalling one) is very close to the short timescale of the system for low α , further showing that the short timescale corresponds to the system without remodelling. As α approaches one from below, the system transitions from the long timescale representing the remodelling effect to it representing the static effect, and the short timescale transitions from representing the non-remodelling exponential effect to capturing the small amount of multiple timescale behaviour inherent in aggregates of discrete cells.

We can also see the effect of varying external forces on the region of biexponentiality

in Figure 7. Increasing the force in the creep experiment increases the region wherein the system acts in a biexponential manner (Figure 7d, displayed as the enclosed region), as well as the maximum coefficient ratio. This is consistent with the experimental data, where the multiple timescale behaviour in the system becomes more pronounced as the force applied on the monolayer is increased (Figure 1a).

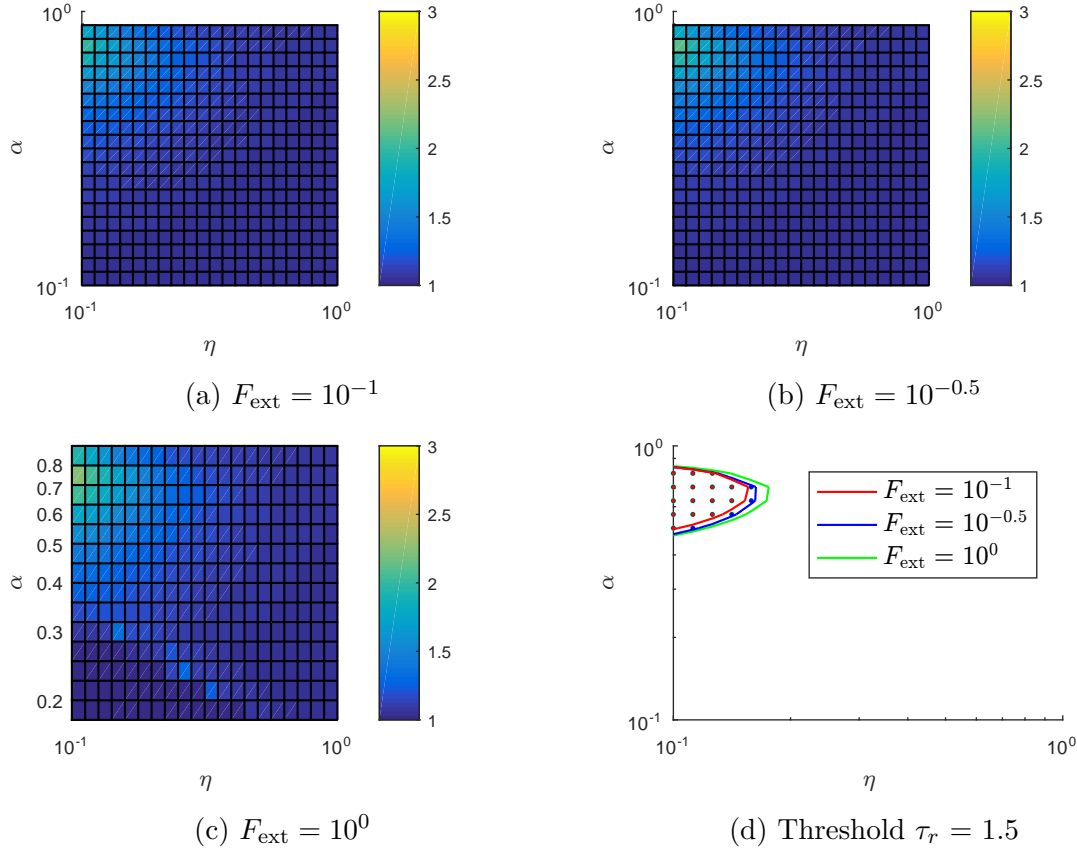


Figure 7: (a,b,c) Surface plots showing varying differences in timescales for different forces in the creep experiment. (d) Compound contour plot showing regions of two exponential behaviour.

Looking at the $F_{\text{ext}} = 10^0$ surface plot in Figure 7c, we see that there is some “noise” in the bottom left hand corner of the plot, where the ratio of coefficients do not act smoothly. If we look at an example of a plot in this region (Figure 8a) we see that in such high force regimes, the data cannot be accurately represented by one or two exponentials. Fitting with a higher amount of exponentials (three in the case of Figure 8), we don’t see any noticeable improvement, indicating that the data in this region cannot be accurately represented by exponentials. Therefore, the surface plot does not show the same “smooth” behaviour as seen in the other plots, due to the metric of two timescale behaviour no longer being applicable.

In these regions of non-smooth behaviour, the strain values are all above four. In the Harris paper, delamination of the monolayer from the testing rods occurred around

a strain value of two, meaning that the simulations with low remodelling ratio and high force are not biologically feasible.

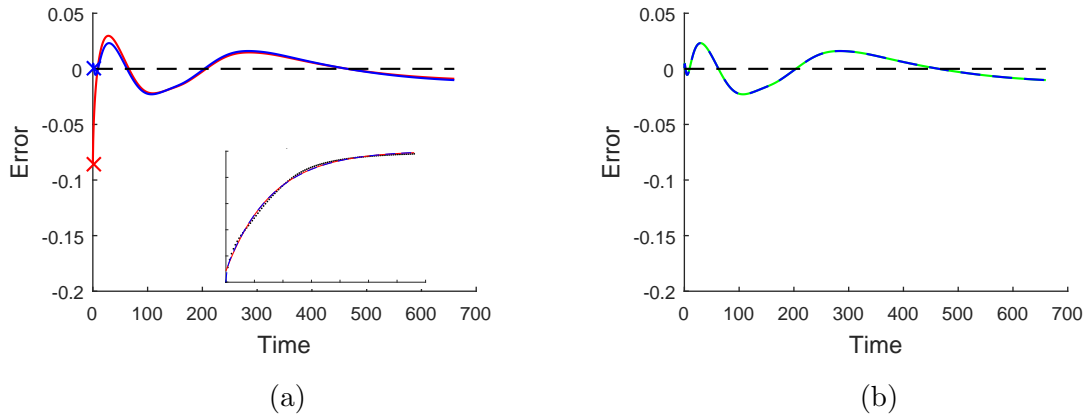


Figure 8: Example errors of a high force/low α simulation. ($\alpha = 10^{-0.6}$, $\eta = 10^{-1}$, $F_{\text{ext}} = 10^0$). (a) One (red) and two (blue) exponential fit errors, with inset strain-time curve. (b) Two (blue) and three (green dashed) exponential fit errors.

3.1.2. Stress Relaxation Experiment In the stress relaxation experiment, we increased the ramp time values T_{ramp} by one order of magnitude, with the values being swept over being 10^1 , $10^{1.5}$ and 10^2 . Some sample stress-time graphs and exponential fits are shown in Figure 9.

One of the main differences in the behaviour of the plots between the creep and stress relaxation experiment is the effect of decreasing α . In the creep experiment, decreasing α , and thus increasing the remodelling component, increases the size of the long timescale. However, in the stress relaxation experiment, after an initial increase in timescale due to the addition of remodelling, further decreasing the value of α has little effect (Figure 9a). Changing the value of η (Figure 9b) has a similar effect to the creep experiment, with decreasing η decreasing the remodelling speed, causing all the timescales to increase, primarily the long timescale τ_{22} .

With regards to two exponential behaviour, we find similar results to the creep experiment. Regions wherein stress-time curves can be comparatively best fitted by two exponentials are areas of high α values and low η values, where there is the largest distinction between the movements of the real and reference state (e.g., Figure 9c), and thus displaying the most multiple timescale behaviour. Simulations further from this region (Figures 9d, 9e) display significantly less multiple timescale behaviour, as can be seen in Figure 9f. We do notice that in Figure 9d has a higher $t = 0$ error for the one exponential curve than Figure 9c, but overall exhibits less two timescale behaviour due to higher initial error in the two exponential fit and generally lower error in the one exponential fit over the given time in Figure 9d. In addition, at least for these parameter regimes, stress-time curves from the stress relaxation experiment tend to be less able to be fitted by a single exponential curve. This is evinced by the greater error values for the

one exponential fit in 9c, greater contributions of the short timescale compared to the creep experiment (generally larger sizes of the black dots in Figures 9a and 9b compared to 6a and 6b) and higher maximum τ_r values in 9f.

In Figure 10 (a,b,c), we see that decreasing T_{ramp} , and thus consequently increasing the strain-rate of loading, increases the maximum magnitude of τ_r observed. This agrees with the experimental data, with multiple timescale behaviour being more prevalent with higher loading strain-rates (Figure 1).

In Figure 10d, we can see that as T_{ramp} decreases the region of biexponential behaviour moves downward, with lower values of α exhibiting multiple time scales. In other words, as the time the strain is ramped over decreases, to compensate for this we need a larger remodelling (lower values of α) component to allow the reference state to sufficiently deviate from equilibrium in the shorter amount of time in order to see a significant presence of multiple timescales.

The change in behaviour as external factors change is a much more dramatic shift for the stress relaxation experiment than the creep experiment, likely due to the inherent external timescale for the stress relaxation experiment (T_{ramp}), and the lack of an external timescale for the creep experiment. We see that for the creep experiment in Figure 7 that a change in force does not significantly change the shape of the region of multiple timescale behaviour, it simply increases the region that this occurs and the magnitude of the coefficient ratio slightly. However, in the stress relaxation experiment in Figure 10, there is a distinct shift in the region of multiple timescale behaviour, and there is a significantly more dramatic increase in the magnitude of multiple timescale behaviour.

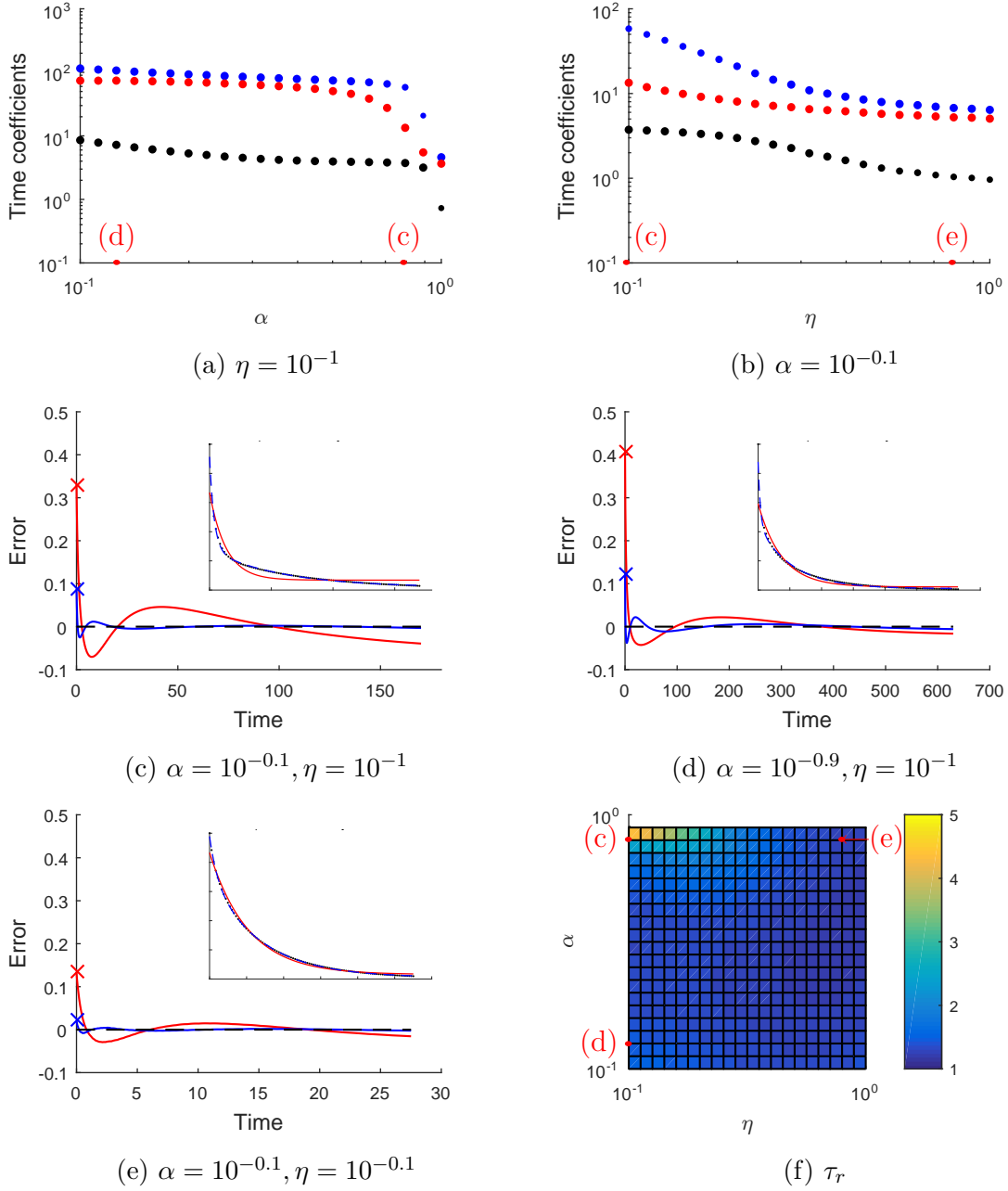


Figure 9: Example timescale differences for the stress relaxation experiment. (a,b) Displays values of τ_1 (red), τ_{21} (black) and τ_{22} (blue), where dot size for τ_{21} and τ_{22} are scaled by B_{21} and B_{22} respectively. (c,d,e) Displays error values for two exponential fit (blue), one exponential fit (red) in comparison to the data (black), with inset stress-time plots showing the original data with the same respective colour scheme. (f) Represents τ_r as surface plot over different η and α values.

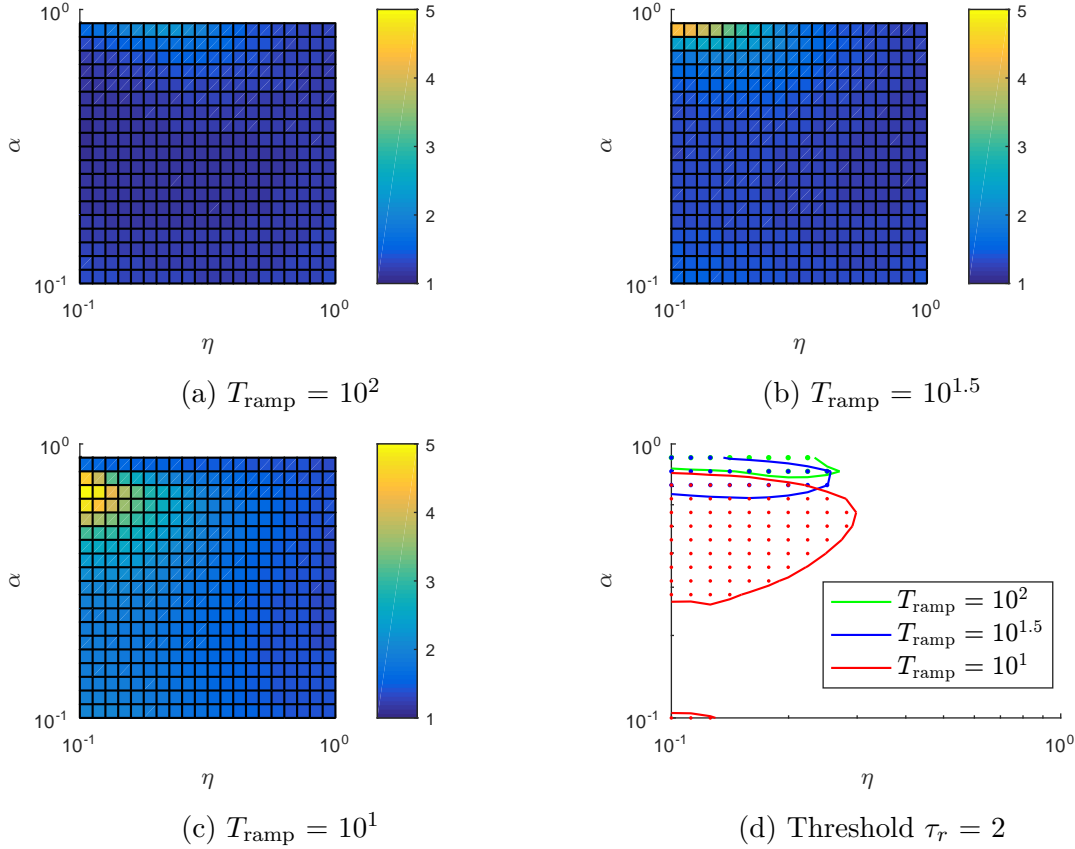


Figure 10: (a,b,c) Surface plots showing varying differences in timescales for different values of T_{ramp} in the stress relaxation experiment. (d) Compound contour plot showing regions of two exponential behaviour.

In Figure 10, in the contour plot displaying $T_{\text{ramp}} = 10^1$, there is a small region of two exponential behaviour in the low η low α region, distinct from the main body of biexponential behaviour. However, the magnitude of the ratio between the two timescales is minimal compared to low η high α region (differing by a scale of around 2.5). The region is visible due to the increased ratio between the two timescale coefficients due to the low ramptime raising this region above the relatively low threshold of τ_r for the higher T_{ramp} values.

3.2. The Addition of Memory Leads to Multiple Time Scales of Remodelling

In order to further investigate the ideas of the time dependency, a form of “memory” was implemented by having the reference state’s dynamics depend not on the current real cell configuration but an average of the intercellular lengths in the real state. The equations of motion for the real cells remain the same as in Equation (4),

$$\frac{d\mathbf{r}_i}{dt} = \sum_{j \in N_i} k(|\mathbf{r}_{ij}| - |\boldsymbol{\rho}_{ij}|)\hat{\mathbf{r}}_{ij} + \mathbf{F}^{\text{applied}}, \quad (9)$$

,

while the equations for the reference state as in Equation (5) now contain an averaging term,

$$\frac{d\boldsymbol{\rho}_i}{dt} = \eta \left(\alpha \sum_{j \in N_i} (|\boldsymbol{\rho}_{ij}| - s_0) + (1 - \alpha) \sum_{j \in N_i} k(|\boldsymbol{\rho}_{ij}| - |\bar{\mathbf{r}}_{ij}|) \right) \hat{\boldsymbol{\rho}}_{ij}, \quad (10)$$

where $\bar{\mathbf{r}}_{ij} = \frac{1}{T_{\text{mem}}} \int_{t-T_{\text{mem}}}^t |\mathbf{r}_{ij}| d\tau$, i.e. it is an average of the previous real lengths, and T_{mem} is the time to average over. $T_{\text{mem}} = 0$ corresponds to the previous memoryless model.

To see the behaviour in the two experiments as we increase the duration of “memory”, we plot surface plots and a compound contour plot for both the creep and stress relaxation experiments in Figures 11 and 12 respectively. From this, we can see the behaviour of the system changing as T_{mem} is varied.

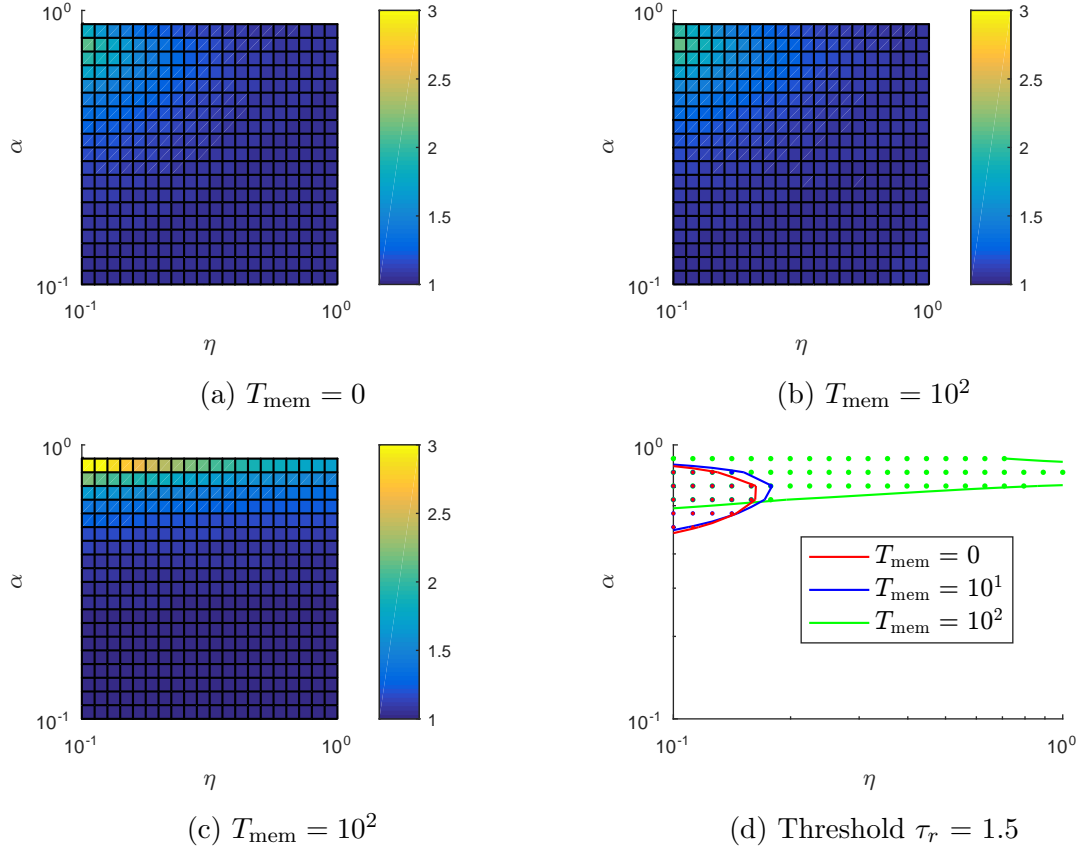


Figure 11: (a,b,c) Surface plots showing varying τ_r values for a sample force ($F_{\text{ext}} = 10^{-0.5}$) in the creep experiment, with differing averaging times. (d) Compound contour plot showing regions of two exponential behaviour.

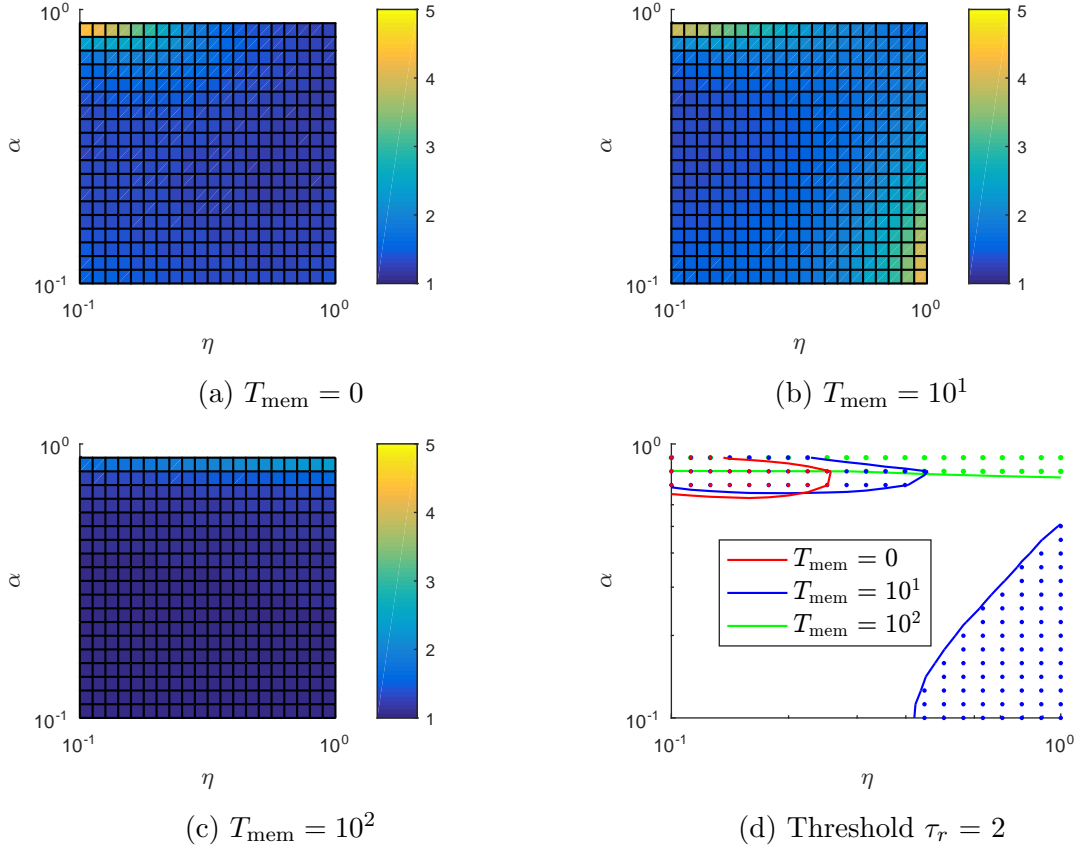


Figure 12: (a,b,c) Surface plots showing varying τ_r values for a sample ramptime ($T_{\text{ramp}} = 10^{1.5}$) in the stress relaxation experiment, with differing averaging times. (d) Compound contour plot showing regions of two exponential behaviour.

We can see an example of this in Figure 11, where we can see that the largest impact that the addition of memory has is increasing the region of two exponential behaviour in the η direction. This is not unexpected, as both T_{mem} and η affect the rate at which information is transferred between the real and reference frames. Therefore, increasing the value of T_{mem} has the effect of allowing the two regions of behaviour to be clearly distinguished even at higher values of η , and so a larger area of the plot exhibits multiple timescale behaviour.

The stress relaxation experiment however exhibits more exotic behaviour than the creep experiment, as we can see in Figure 12. Any timescales in the creep experiment come from the model, and therefore interactions between the averaging with the creep experiment are not that complex. However, in the stress relaxation experiment, there is an additional timescale involved with the presence of the variable T_{ramp} .

At low values of T_{mem} , we get similar behaviour as the creep experiment, with the upper left region of the plot (values of α close to 1, low values of η) being the primary region of multiple timescale behaviour. However, as T_{mem} increases, a ‘lip’ at the bottom right hand part of the plot arises (high η , low α) where the presence of delay introduces a new region of biexponential behaviour. However, as the value of T_{mem}

continues to increase, we see that the two timescale regions decrease again, to a similar behaviour as seen in the creep experiment. This suggests that as the averaging time increases, the averaging (vs non-averaging) component becomes the dominant effect in this region, and so the system goes back to displaying predominantly one timescale.

We can see examples of this in Figure 13. Increasing the value of T_{mem} initially introduces regions where there are two distinct timescales, but further increases of the averaging time result in curves that cannot be accurately modelled by two or more exponentials. Therefore, we will get biexponential behaviour from two different sources; one from the high α low η region, being relatively unaffected by the averaging time T_{mem} and is similar to the creep experiment, and another due to the interaction of the averaging on the system as the strain is applied. This second region is much more complicated due to the multiple competing factors, and is not a two or three timescale region.

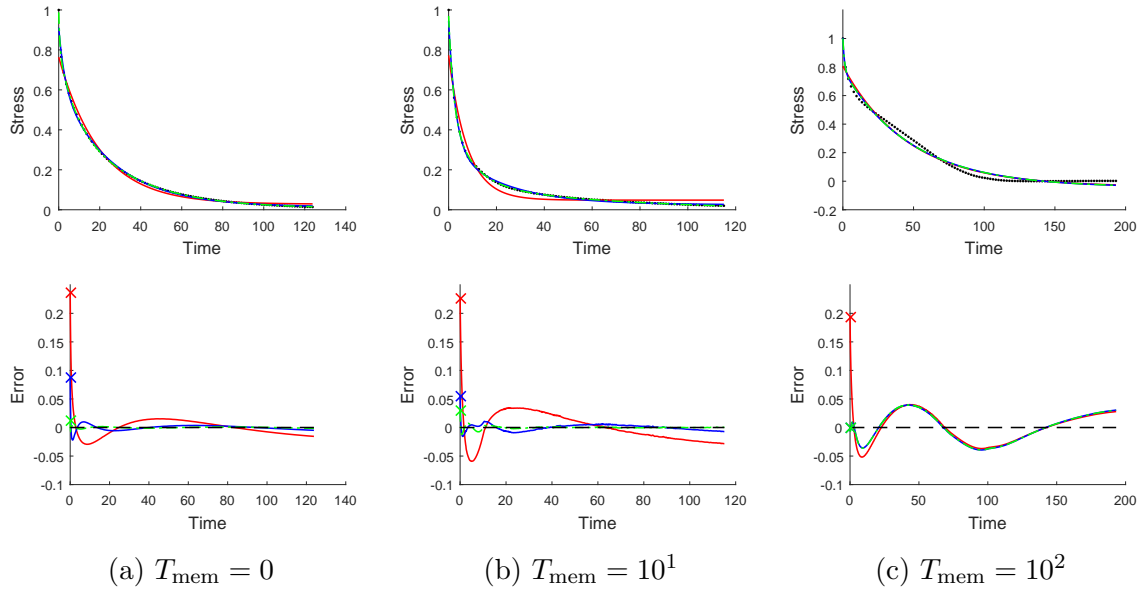


Figure 13: Top: Example stress-time plots from region of varying biexponentiality as the averaging time T_{mem} varies. Bottom: Differences in the exponential approximations with the original data, with red being one, blue being two and green being three exponential fits.

4. Discussion

In this paper, we implemented a dynamic reference state in an off lattice discrete cell model in an attempt to represent cellular remodelling, in order to see multiple timescale behaviour as observed experimentally [7]. Parameter sweeps over the remodelling parameters, the remodelling ratio α and remodelling rate η , were undertaken over two *in silico* experiments, a creep experiment and a stress relaxation experiment. Strain and stress curves were then fitted with both one and two exponential fits, and the

characteristic timescales of these exponentials were then compared to determine the presence of multiple timescale behaviour.

It was found that the greatest presence of two exponential behaviour, determined by high ratios of timescales for the two fits, was in regions of high remodelling ratio and low remodelling rate, where interactions between the two states were most distinct and separated. Adding in the presence of time delayed averaging increased the areas of two exponential behaviour, but the increased complexity also introduced regions wherein sum of exponential approximations were not appropriate fits.

From this data, we saw the addition of the reference state in these parameter regimes mimicked the effects seen experimentally, with two clear timescales being observed that were not present in the model with a static reference frame. We also found that the extent of this multiple timescale behaviour was more pronounced in response to larger forces and higher loading strain-rates for both the creep and stress relaxation experiments respectively, which is consistent with the data observed experimentally.

5. Future Work

5.1. Alternate Cell Models

In this paper, all of the simulations and parameter sweeps were done with a linear spring cell centre model, one of the simpler multicellular models. To further explore these ideas, reference cells could also be added to a vertex based model [12]. In this method, one could potentially add time dependency to the discrete cell model with a vertex based reference state instead of a cell centre based reference state. Information between the real and reference states can then be transferred between each other based upon the properties of the cell, such as cell area, cell circumference or potential other cell properties.

5.2. Multiple Reference States

In the model described in the paper, the reference state bases its dynamics on both the position of the real cells, as well as a set of static parameters. However, the reference state could have its own, higher level, reference state in order to allow its parameters to change. This would allow the effects of another set of cell components with their own differing remodelling timescales to be implemented, with their own sets of remodelling rates and remodelling ratios.

This process could theoretically be repeated *ad infinitum* (subject to computational constraints), with each reference frame having another reference frame in order to simulate as many timescales, and inherently the presence of biological processes, as necessary in order to accurately model the monolayer behaviour.

5.3. Three Dimensional Modelling

This model has a natural extension to three dimensions. All of the equations of motion for the cells will remain the same, but with the locations of the cells and the connectivity between cells being based upon three dimensional cell configurations. Such an extension should allow the framework to be used in more complicated biological systems than the epithelial monolayers discussed in this paper, in order to incorporate higher order timescale effects into such systems.

5.4. Monolayer Restructuring with Reference State

Often we want the connectivity of the cells to change, due to birth or death processes of cells, or rearrangement of cells due to external forces [5]. Birth processes generally involve the division of a mother cell into two daughter cells, requiring the connectivity of the other cells to shift in response to this. Forces acting on cells can cause vertices to become too close, or for cells to intersect, requiring locations and connections to be created or shifted.

A reference state, at least in the current formulation, requires the same connectivity between the two states for the appropriate parameter information to be transferred. Therefore, how the reference state reacts to these changes in connectivity is paramount if these operations are implemented. In response to any change in the real state, evidently any change in connectivity needs to be emulated in the reference state. However, the method to implement this in the other direction, from reference state to real state, is not immediately clear. It may be appropriate for the reference state to undergo changes in connectivity, due to intercellular distances being outside the normal range, for example. However, any change in connectivity would have to be replicated in the real state in this model, potentially in cases where the real state is in no need of such changes. Work would need to be done to see the impact of differing choices for the restructuring behaviour with a reference state, in order to find the optimal choice of model implementation.

In addition, work would need to be done to find the how one would implement averaging effects in a model with changing connectivity. Possible choices of past distances between cells for the purpose of calculating average intercellular distances for a new cell connection could be inheriting these values from previous or surrounding intercellular bonds, or assuming a static equilibrium value of the new bond's length.

5.5. Implementation Details of Creep and Stress Relaxation Experiment

In both the creep and stress relaxation experiment simulations in the cell centre model, the left hand side of the cell monolayers are held fixed via setting the all of the derivatives acting upon these cells to zero. For the right hand, extra care needs to be taken for the *in silico* experiment to match the experiments done in Harris et al. [7]. In these experiments, the sides of the monolayer are fixed to straight rods that are moved or

held fixed, depending on the experiment and side. Therefore, the final column of cells on the right hand side of the monolayer are held in fixed relative position to each other.

For the creep experiment, in order to implement this in the simulations, all vertical forces on this right hand are discarded, effectively being absorbed by the rod the monolayers are connected to. For the horizontal forces, the forces on the cells in the final column are averaged over all of the cells in this column, allowing the relative positions of the cells to stay fixed.

In the stress relaxation experiment, in the initial period where the strain is increasing linearly, the right hand column of cells are moved in concert with each other horizontally in accordance with the strain rate. In the relaxation component of the experiment, these cells are then held fixed. Again, in both stages, the vertical components of the force on these cells are discarded to keep the cells in fixed relative position.

5.6. Equilibration Time Calculation

In order to plot and analyse graphs, an appropriate time interval is needed to compare graphs of different parameters. The simulations were initially run over a long period of time to give sufficient time for the systems to equilibrate. For the creep experiment, the time it took for 90% of the creep to occur was found, and twice this value was used as the final time for each simulation.

This was slightly more involved in the stress relaxation experiment. The long term stress is completely determined by the value of α , as this is the only parameter in the system that determines the structure of the system at equilibrium; this occurs in both the creep and stress relaxation experiments. In the creep experiment, the initial value of the creep is always one, meaning choosing a 90% point is simple. However, in the stress relaxation experiment, the initial (and maximum) stress is dependent on both η and T_{mem} . In order to get a non-biased initial value for the stress dependent only on alpha (not η or T_{mem}), we want an instant remodelling of the system to be used as a reference. This was implemented by running an extra simulation, for each $T_{\text{ramp}}-\alpha$ pair, with $T = 0$ and a very high value of η , $\eta = 1000$, three orders of magnitude higher than any values used in the simulation, in order to approach instant remodelling. The initial stress of this simulation was recorded, and two times the 90% point between the initial and final values of stress was used in order to calculate a final time.

Decreasing α increases the extent of the remodelling, and decreasing η decreases the speed of the remodelling, so we expect that decreasing either of these parameters will increase the length of time taken in order to equilibrate, which we can see as in Figure 14.

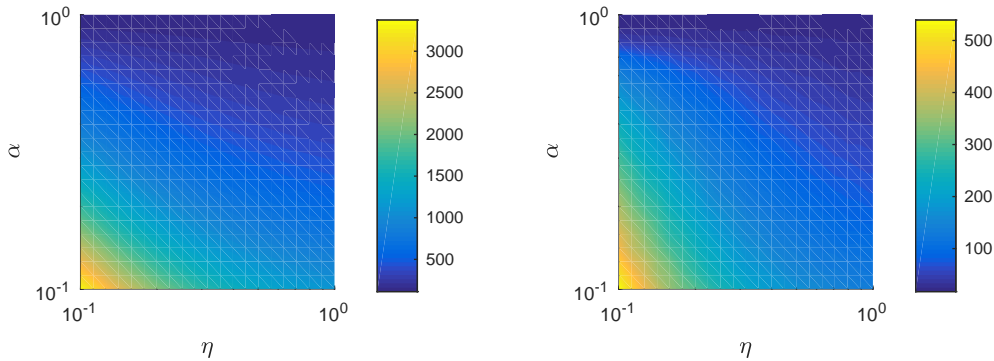


Figure 14: Time to reach equilibrium as a surface plot over η and α for the creep (left) and stress relaxation experiments (right), with $T_{\text{mem}} = 0$.

References

- [1] G Wayne Brodland. Computational modeling of cell sorting, tissue engulfment, and related phenomena: A review. *Applied Mechanics Reviews*, 57(1):47–76, 2004.
- [2] B. Delaunay. Sur la sphère vide. *Izv. Akad. Nauk SSSR, Otdelenie Matematicheskii i Estestvennyka Nauk*, 7:793–800, 1934.
- [3] Dirk Drasdo. Buckling instabilities of one-layered growing tissues. *Physical Review Letters*, 84(18):4244, 2000.
- [4] Sara-Jane Dunn, Inke S Nähkhe, and James M Osborne. Computational models reveal a passive mechanism for cell migration in the crypt. *PLoS One*, 8(11):e80516, 2013.
- [5] Alexander G. Fletcher, James M. Osborne, Philip K. Maini, and David J. Gavaghan. Implementing vertex dynamics models of cell populations in biology within a consistent computational framework. *Progress in Biophysics and Molecular Biology*, 2013.
- [6] Yuan-Cheng Fung. Biomechanics. *Applied Mechanics Reviews*, 38(10):1251–1255, 1985.
- [7] Andrew R. Harris, Loic Peter, Julien Bellis, Buzz Baum, Alexandre J. Kablaa, and Guillaume T. Charras. Characterizing the mechanics of cultured cell monolayers. *PNAS*, 2012.
- [8] H. Honda, Y. Ogita, S. Higuchi, and K. Kani. Cell movements in a living mammalian tissue: Long-term observation of individual cells in wounded corneal endothelia of cats. *Journal of Morphology*, 174(1):25–39, 1982.
- [9] Gareth Wyn Jones and S. Jonathan Chapman. Modeling growth in biological materials. *SIAM Rev.*, 54(1):52–118, February 2012.
- [10] Harvey F. Lodish. *Molecular Cell Biology*. New York : W.H. Freeman and Co., 2013., 2013.

- [11] José J Muñoz and Santiago Albo. Physiology-based model of cell viscoelasticity. *Physical Review E*, 88(1):012708, 2013.
- [12] P Pathmanathan, J Cooper, A Fletcher, G Mirams, P Murray, J Osborne, J Pitt-Francis, A Walter, and S J Chapman. A computational study of discrete mechanical tissue models. *Physical Biology*, 6(3):036001, 2009.
- [13] Matteo Rauzi, Pascale Verant, Thomas Lecuit, and Pierre-Francois Lenne. Nature and anisotropy of cortical forces orienting drosophila tissue morphogenesis. *Nature Cell Biology*, 10(12):1401, 2008.
- [14] Esra Roan and Christopher M Waters. What do we know about mechanical strain in lung alveoli? *American Journal of Physiology-Lung Cellular and Molecular Physiology*, 301(5):L625–L635, 2011.